







# Physics-Based Electrothermal Stress Evaluation Approach of IGBT Modules Combined With Artificial Neural Network Model

YIPING LU <sup>1</sup> (Student Member, IEEE), ENYAO XIANG <sup>1</sup>, ANKANG ZHU <sup>2,3</sup>, HONGYI GAO <sup>2,3</sup>,  
HAOZE LUO <sup>2,3</sup> (Senior Member, IEEE), HUAN YANG <sup>1</sup> (Member, IEEE),  
AND RONGXIANG ZHAO<sup>1</sup> (Member, IEEE)

<sup>1</sup>Zhejiang Provincial Key Laboratory of Electrical Machine Systems and the College of Electrical Engineering, Zhejiang University, Hangzhou 310058, China

<sup>2</sup>ZJU-Hangzhou Global Scientific and Technological Innovation Center, Hangzhou 310058, China

<sup>3</sup>College of Electrical Engineering, Zhejiang University, Hangzhou 310058, China

CORRESPONDING AUTHOR: HAOZE LUO (e-mail: haozeluo@zju.edu.cn)

This work was supported in part by the National Natural Science Foundation of China under Grant 52177062, in part by the Pioneer and Leading Goose R&D Program of Zhejiang under Grant 2022C01094, and in part by the National Key Research and Development Program of China under Grant 2022YFE0138400.

**ABSTRACT** Due to the disparate timescale behavior in the electrical and thermal aspects, achieving a balance between simulation efficiency and accuracy in electrothermal analysis of insulated gate bipolar transistor (IGBT) modules has been a challenging task. A physical-based electrothermal stress evaluation approach combining with artificial neural network (ANN) model is proposed in this article, which significantly improves performance in circuit simulation. The training data for ANN models are derived from the Hefner physical model, a well-established model integrated in Saber. By re-expressing the Hefner model using MATLAB scripts, high-precision data can be efficiently obtained. Double-pulse experiments show that the switching transient characterized by the Hefner model have high precision, with an error within 5% compared to the experimental data. Additionally, the transient behavior of IGBT devices is further described by a two-layer feed-forward ANN, trained using datasets obtained by varying parasitic or operating parameters in the re-expressed Hefner model. Combining the physical model with the ANN models, the proposed approach can simulate not only transient electrical behavior but also long-term thermal behavior with accurate switching energy. This approach has been implemented in MATLAB/Simulink and verified with Saber for system-level circuit simulation. The electrothermal stress evaluation results show that the simulation efficiency is significantly improved (180 times faster than Saber under the simulation settings in this article), while maintaining high precision, and the error is within 2.5%. Experimental results also validate the accuracy of proposed model in predicting the voltage and current stress, with a maximum error of 1.5%.

**INDEX TERMS** Artificial neural network (ANN), electrothermal stress, physical model, insulated gate bipolar transistor (IGBT).

## I. INTRODUCTION

Insulated gate bipolar transistor (IGBT) modules have been widely used in the new energy power electronic systems (PES), such as electric vehicles (EVs), smart grid, photovoltaic and wind energy generation [1], [2]. According to industry surveys, IGBT modules have a much

shorter lifespan than the whole PES with larger power ratings due to unforeseen severe electrothermal stress in filed applications [3]. In order to avoid the “over-margin” phenomenon in device selection, it is essential for PES designers to accurately obtain the electrothermal stress of IGBT modules during the design phase. However, a test

platform is typically associated with significant resource investment. Moreover, it is also challenging for commercial circuit simulation software to obtain electrothermal stresses of IGBT modules efficiently and accurately. The commonly used simulation software mainly consists of two technical routes: device model and look-up table (LUT) based model.

For the first, the compact device model is generally supported by the device manufacturer and can be divided into the physical model and the behavioral model. For the former one, integrated in the Saber software, the Hefner model [4], [5], [6] is the most classic physical model, and its assumptions of non-quasi-static approximation, bipolar transport, and large base injection are still widely used today. Additionally, the nonlinear capacitances can be fully considered in this model to obtain accurate switching transient process [6]. Further, the two-dimensional Hefner model was extended to a three-dimensional model by Kuang Sheng et al. in [7]. The Hefner model is improved for the physical modeling of high-power IGBTs in [8]. As another mature physical model, Kraus model has been implemented in Spice language and provided by module manufacturers such as Infineon [9], Mitsubishi [10] and Toshiba [11]. The supporting commercial simulation software mainly includes LTspice, Pspice and SIMetrix/ SIMPLIS [12], [13], [14]. Physical models undoubtedly own the better simulation performance for electrical stress. However, the nonlinear model involved in solving the carrier distribution seriously reduces the simulation efficiency. For the latter one, hierarchical behavioral model has been integrated in the ANSYS SImplorer [15] to satisfy the demands for different simulation scenarios. Besides, another behavioral model [16] based on piecewise analytical transient is applied in the PSIM and DSIM software, which demonstrates extremely high simulation efficiency in megawatt-scale PES combined with a specific discrete-state event-driven method [17]. However, simplified description of switching behavior cannot maintain high simulation accuracy under varying operating conditions.

For the second, LUT-based model has been normally used in PLECS [18], which employs an ideal representation that omits switching transients and enables calculating power loss and junction temperature characteristics for long-term mission profiles with a higher efficiency. However, due to the limited number of values in LUTs (typically collected by datasheets), it may not cover all operating conditions in the field, e.g., voltage, current, temperature and gate resistance, which limits the accuracy of thermal stress. More interpolation is added in [19] to improve its accuracy but the simulation speed will decrease.

As shown in Table 1, a survey has been fully conducted in this article. Mainly due to the different timescales of electrical and thermal behaviors, the commercial circuit simulation software has not been able to reconcile the trade-off between accuracy and efficiency in electrothermal simulation. Furthermore, while various methods have been devoted to calculate the electrical stress [20] or thermal stress [21], [22] under different time scales, these two aspects are rarely considered simultaneously, which is not suitable to designing the PES within a safety margin and introduces the problem of

TABLE 1. Comparison on Commercial Circuit Simulation Software

IGBT model	Type	Software	Electrical behavior	Thermal behavior	Efficiency	Ref.	
Device model	Physical	Hefner	Saber	★★★★	★	★★	[4]-[6]
		Kraus	LTspice			★	[12]
			Pspice	★★★★	★	★	[13]
		SIMetrix			★★	[14]	
	Behavioral	Hierarchical	ANSYS SImplorer	★★★	★★	★★	[15]
Piecewise analytical		PSIM /DSIM	★★	★★★★	★★★★	[16]-[17]	
LUT based model	Ideal	PLECS	×	★★★★	★★★★	[18]	

★★★★ -- Excellent    ★★★ -- Good    ★★ -- General    ★ -- Poor    × -- none

“over-margin”. Therefore, this article proposes an optimized stress evaluation approach combined with ANN model to achieve an accurate and efficient electrothermal assessment of IGBT modules. Owing to their high robustness, the ANN models can well reflect the mapping relationship between unstructured input and output through training the sample dataset [23]. Therefore, a two-layer feed-forward ANN is adopted in this article instead of LUTs, which contains key electrothermal stress information, e.g., switching energy, current and voltage overshoot. Besides, the training data used for ANN models is derived from the Hefner physical model based on the movement of carriers, which is widely used in switching transient modeling of IGBT device as a mature and accurate model [6], [7], [8]. It is worth mentioning that MATLAB scripts are used to describe the movement of carriers and realize the physics-based Hefner model, which provides higher acquisition efficiency of electrothermal stress information instead of Saber.

The rest of this article is organized as follows: Section II introduces the principle of the physics-based Hefner model and its re-expression in MATLAB script. Section III presents a two-step parameter extraction method for the Hefner model. The verification of the switching transient with experiments is also given in this part. Section IV details the modeling and training processes of the ANN models, which takes the electrothermal stress data obtained in Section II as input. Based on the above work, the complete implementation process of the proposed electrothermal stress evaluation approach in Simulink and its validation are also presented. Finally, Section V provides a conclusion.

## II. RE-EXPRESSION ON HEFNER PHYSICAL MODEL

The physics-based Hefner model is a well-established and accurate representation for IGBT devices and therefore an ideal data source for training ANN models. Nonetheless, as integrated in Saber, the Hefner model may not support large-scale data collection, as the simulation waveform cannot automatically generate the required data. To address this issue, the principle of Hefner model is analyzed and re-expressed using MATLAB, which enables automatic processing on simulation waveform. This article focuses on the Infineon

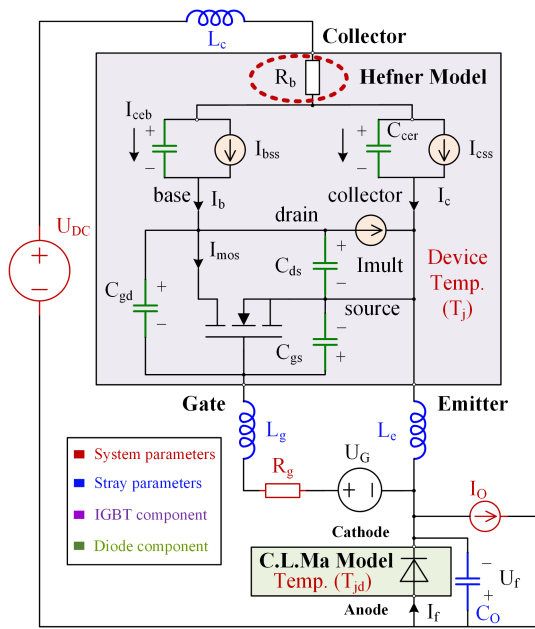


**FIGURE 1.** Equivalent circuit diagram of IGBT Hefner model.

FS820R08A6P2B, a high-power IGBT module with a rating voltage of 750V and a current of 820A.

Fig. 1 shows the equivalent circuit diagram of an IGBT module during the switching transient process, incorporating the C.L.Ma model proposed for power diodes in [24], [25]. The operating parameters that describe the behavior of the device during the switch transient, includes the DC-bus voltage ( $U_{dc}$ ), bridge arm output current ( $I_o$ ), gate resistor ( $R_g$ ), junction temperature of IGBT ( $T_j$ ), and Diode ( $T_{jd}$ ). In addition, parasitic parameters including of package and system circuit are also considered, e.g., common emitter inductance ( $L_e$ ), gate inductance ( $L_g$ ), collector inductance ( $L_c$ ) and parasitic capacitance ( $C_o$ ) of Diode.

Fig. 1 provides the equivalent circuit diagram, and the relationship between gate current  $I_g$  and gate-source voltage  $U_{gs}$  (i.e., gate-emitter voltage  $U_{ge}$ ) is described as (1).

$$I_g = C_{gs} \frac{dU_{gs}}{dt} + C_{gd} \frac{dU_{gd}}{dt} \quad (1)$$

$$U_G = (L_g + L_e) \frac{dI_g}{dt} + L_e \frac{dI_g}{dt} + R_g \cdot I_g + U_{ge} \quad (2)$$

Where  $U_G$  is the driving voltage,  $C_{gs}$  and  $C_{gd}$  are the gate-source capacitance gate-drain capacitance respectively, and  $I_{ce}$  is the collector-emitter current and can be expressed as (3).

$$I_{ce} = I_b + I_c = I_{bss} + \frac{dQ}{dt} + I_{css} + C_{cer} \frac{dU_{ds}}{dt} \quad (3)$$

Where  $I_c$  is the collector current,  $I_{css}$  is the collector steady-state current,  $I_b$  is the base current,  $I_{bss}$  is the base steady-state current,  $Q$  is the instantaneous excess carrier base charge, which describes the carrier density in the transistor channel Distribution.  $C_{cer}$  is the channel-substrate capacitance of the transistor, also known as MOS capacitance. It describes the capacitive relationship between the channel of a transistor and

the substrate. In the MOSFET section, the base current  $I_b$  can be expressed as (4).

$$I_b = C_{ds} \frac{dU_{gs}}{dt} + I_{mult} + I_{mos} - (C_{ds} + C_{gd}) \frac{dU_{gd}}{dt} \quad (4)$$

Where  $I_{mos}$  is the channel current,  $C_{ds}$  is the drain-source capacitance, and avalanche multiplication current  $I_{mult}$  are related. In addition, the relationship between the voltage and current in the entire loop consisting of the IGBT component, diode component and DC bus can be expressed as (5) and (6).

$$U_{dc} + U_f = \overbrace{U_{ds} + V_{ebq} + I_{ce} \cdot R_b}^{U_{ce}} + (L_c + L_e) \frac{dI_{ce}}{dt} \quad (5)$$

$$I_o = I_{ce} + I_f + C_o \frac{dU_f}{dt} \quad (6)$$

Where  $U_f$  is the voltage across the diode, collector-emitter voltage  $U_{ce}$  is calculated by the voltage of drain-source  $U_{ds}$ , the emitter-base capacitance  $V_{ebq}$  and the base resistor  $R_b$ . Additionally,  $R_b$  is modulated by the conductance. Further,  $I_f$  represents the Diode current and is calculated in (7) [25].

$$I_f = \frac{q_E - q_M}{T_M} \quad (7)$$

Where  $q_E$  represents the charge caused by the diffusion current in the reverse bias, which is a controlled charge variable in C.L.Ma model.  $q_M$  represents the charge caused by the diffusion current in the forward bias.  $T_M$  represents the diffusion time constant. The relationship between them are described in (8) and (9).

$$0 = \frac{dq_M}{dt} + \frac{q_M}{\tau} - \frac{q_E - q_M}{T_M} \quad (8)$$

$$q_E = I_s \cdot \tau \cdot \left[ \exp\left(\frac{U_f}{2V_T}\right) - 1 \right] \quad (9)$$

As (1)–(9) that describe the switching transient process involve nonlinear differential as well as algebraic equations, obtaining the derivatives of various variables with respect to time requires a numerical method. In this study, the backward difference method is employed to approximate these derivatives. This method enables converting (1)–(9) into specific nonlinear equations. Then, the MATLAB built-in function *fsolve* is called at each time step to calculate the variables. Moreover, since the convergence of function *fsolve* shows strong sensitivity in the initial value setting, the solution in the previous shot is utilized as the solution initial value for the next step. in this re-expressed model.

Additionally, it is essential to incorporate second-order effects that are not included in the phenomenological circuit [6]. Therefore, after the solution is completed at each time step, the component of base-collector space charge caused by velocity saturation  $N_{sat}$  is updated using (10). The reciprocal component of mobility  $\mu_c$  due to carrier-carrier scattering is also updated using (11).

$$N_{sat} = \frac{I_c}{qA v_{psat}} - \frac{I_{mos}}{qA v_{nsat}} \quad (10)$$

$$\frac{1}{\mu_c} = \left[ dp \cdot \ln \left( 1 + \alpha_2 \cdot (dp)^{-\frac{2}{3}} \right) \right] / \alpha_1 \quad (11)$$

Where  $A$  is the active die area,  $dp$  is the average carrier concentration of the base region,  $v_{psat}$  and  $v_{nsat}$  are two parameters describing the saturation speed of silicon materials at different doping concentration and temperatures.  $\alpha_1$  and  $\alpha_2$  are parameters used to describe the behavior of transistors, which are related to material properties and change with temperature. Both of them can be determined by empirical values or fitting experimental data [6].

In addition, once the calculation process for all time steps is finished, the stored variables are automatically processed and certain characteristic values of the switching transients is calculated, which include the turn-on energy ( $E_{on}$ ), turn-off energy ( $E_{off}$ ), reverse recovery energy ( $E_{rr}$ ), turn-on delay time ( $t_{don}$ ), turn-off delay time ( $t_{doff}$ ), rise time ( $t_r$ ) and fall time ( $t_f$ ). In order to verify the effectiveness of the re-expressed model, the extraction of these eigenvalues is in accordance with the definition in the datasheet. For example, the integral range of turn-on energy  $E_{on}$  starts at the point of 10% of  $I_{ce}$  and ends at the point of 2% of  $U_{ce}$ .

### III. MULTI-STEP PARAMETER EXTRACTION WITH FORMAL OPTIMIZATION

In this section, the results of parameter extraction are provided. In addition, some key parameters are determined by doing few experiments for improving its accuracy.

#### A. PARAMETER EXTRACTION FOR C.L. MA MODEL

According to the above analysis, three parameters need to be extracted in the C. L. Ma model, e.g.,  $\tau$ ,  $I_s$  and  $T_M$ . Based on the data provided in the module datasheet [26], these parameters are extracted by (12)–(14).

$$\tau_{rr} = (t_{rr} - I_{rr}/a) \quad (12)$$

Where  $t_{rr}$  represents the reverse recovery time,  $a$  is the current decay rate. Both of them are provided in the datasheet.

$$I_{rr} = a \cdot (\tau - \tau_{rr}) [1 - \exp(-(I_{rr} + I_0)/(a \cdot \tau))] \quad (13)$$

Where  $I_{rr}$  is the peak reverse recovery current provided in the datasheet. Combined with the value of  $I_{rr}$ ,  $\tau$  can be extracted by solving (13). Moreover, the value of  $T_M$  can be determined by the following:

$$\frac{1}{T_M} = \frac{1}{\tau_{rr}} - \frac{1}{\tau} \quad (14)$$

Finally,  $I_s$  can be determined by (15), where  $U_F$  and  $I_F$  are the nominal data of forward voltage and forward current that presented in the datasheet, respectively.

$$I_s = \left( 1 + \frac{T_M}{\tau} \right) \cdot \frac{I_F}{\exp\left(\frac{U_F}{2V_T} - \frac{T_M}{\tau}\right)} \quad (15)$$

Based on the above analysis, the results of the extracted three parameters  $\tau$ ,  $I_s$  and  $T_M$  are given in Table 2.

TABLE 2. Parameter Extraction Result for C.L.MA Model

Test conditions	Symbols/Units	Values	
Device temperature	$T_{jd}$ (°C)	25	150
Current decay rate	$a$ (A/ $\mu$ s)	5000	5000
Reverse recovery time	$t_{rr}$ (ns)	120	210
Reverse recovery current	$I_{rr}$ (A)	250	350
Bridge arm output current	$I_o$ (A)	450	450
Nominal forward current /voltage	$I_F$ (A) / $U_F$ (V)	450/1.45	450/1.30
Extracted parameters by Eq. (12)-(14)	$\tau$ (ns)	115.4	223.1
	$I_s$ (A)	1.6e-12	1.7e-12
	$T_M$ (ns)	89.8	184.5

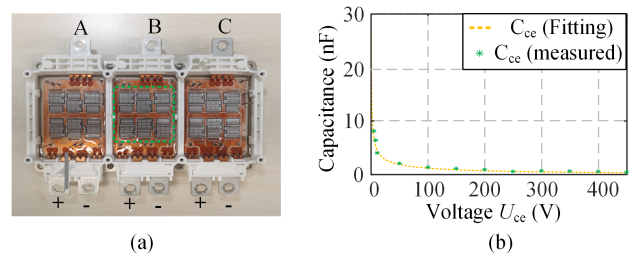


FIGURE 2. Initial parameter extraction for area. (a) Device active area  $A$ . (b) Drain-source overlap area  $A_{ds}$ .

#### B. INITIAL PARAMETER EXTRACTION FOR HEFNER MODEL

- 1) First, the base doping concentration  $N_B$  and base width  $W_B$  can be obtained from the forward breakdown voltage of IGBT device, which is determined by the avalanche breakdown of abrupt punch-through diode [27].

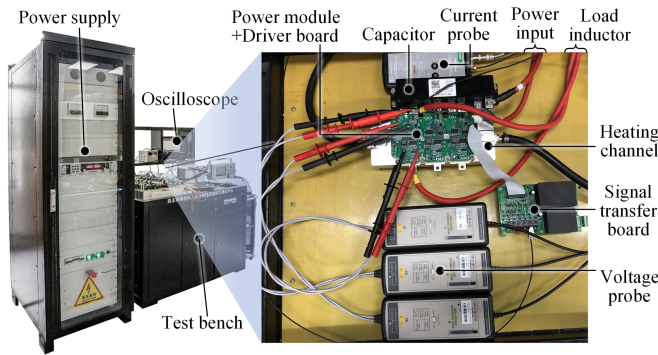
$$\begin{cases} BV_{PT} = E_{c-si} W_B - \frac{qN_B}{2\epsilon_{si}} W_B^2 \\ E_{c-si} = 4010N_B^{0.125} \end{cases} \quad (16)$$

Where  $BV_{PT}$  refers to the breakdown voltage value from the datasheet with an additional margin of approximately 300V.  $E_{c-si}$  represents the critical electric field for breakdown, which corresponds to  $N_D$  in the lightly doped portion of the N-base region, which can be presented by (16).

- 1) Second, as shown in Fig. 2, the active die area  $A$  can be measured directly through the package. Considering the voltage dependence characteristics with terminal capacitors, the drain-source overlap area  $A_{ds}$  is obtained from the measured  $C_{CE}$  ( $U_{ce}$ ) by using planar capacitor formula.
- 2) After  $A$  and  $A_{ds}$  are determined, the gate-drain overlap area  $A_{gd}$  and oxide layer capacitance  $C_{oxd}$  can be calculated, here the thickness  $t_{ox}$  of silicon oxide is set as 0.1  $\mu$ m.
- 3) According to the I-V characteristics  $I_{ce}$  ( $U_{ge}, U_{ce}$ ) provided in the datasheet, the  $K_{Pin}$  (triode region factor) can be calculated by the cut-off point between the

**TABLE 3. Initial Parameter Extraction Process for Hefner Model**

Step	Using Equation	Source data	Extracted Para.
1	$\begin{cases} BV_{PT} = E_{c-si} W_B - \frac{qN_B}{2\epsilon_{si}} W_B^2 \\ E_{c-si} = 4010N_B^{0.125} \end{cases}$	$BV_{PT}$	$N_B=27.4 \times 10^{13} \text{cm}^3$ $W_B=0.0061 \text{cm}$
2	$\begin{cases} W_{dsj} = \sqrt{2\epsilon_{si}(U_{ce} + 0.6) / (qN_B)} \\ A_{ds} = C_{ce} \cdot W_{dsj} / \epsilon_{si} \end{cases}$	$C_{ce}(U_{ce})$	$A=3.1 \text{cm}^2$ , $A_{ds}=1.84 \text{cm}^2$
3	$\begin{cases} A_{gd} = A - A_{ds} \\ C_{oxd} = A_{gd} \epsilon_{\text{SiO}_2} / t_{ox} \end{cases}$	$A, A_{ds}$	$A_{gd}=1.26 \text{cm}^2$ $C_{oxd}=35.4 \text{nF}$
4	$\begin{cases} I_{mos} = 0.85 \cdot I_{cc} \\ I_{mos} = 0.85 \frac{K_{psat}(U_{ge} - V_T)^2}{(1 + \theta(U_{ge} - V_T))} \\ U_{ce} - V_{bi-pin} = (U_{ge} - V_T) / K_{plin} \end{cases}$	$I_{cc}(U_{ge}, U_{ce})$	$V_T=5.8 \text{V}$ $\theta=0.016$ $K_{psat}=102.3$ $K_{plin}=12.84$
5	$\frac{d \ln I_T}{dt} = \frac{dI_T/d}{I_T} = -\frac{1}{\tau_{HL}} \left(1 + \frac{I_T}{I_k}\right)$	On/off Test	$\tau_{HL}=0.08 \mu\text{s}$


**FIGURE 3. Experimental setup of double-pulse dynamic test platform.**

linear region and saturation region. subsequently,  $V_T$ ,  $\theta$  (transverse field trans-conductance factor) and  $K_{P_{sat}}$  (trans-conductance factor) can be obtained from the  $I_{mos}$  formula [28].

- 4) Last, the base high-level lifetime  $\tau_{HL}$  can be extracted by analyzing the decay rate of IGBT tail currents, which can be measured under different drain currents  $I_T$  [28].

The above detailed steps and used equations are listed as Table 3, five steps are summarized for extracting the initial parameters of Hefner IGBT model. As shown in Fig. 3, it is worth mentioning that the measurement on the capacitance as well as tail current decay rate has been finished with the double-pulse dynamic test platform and the power device analyzer curve tracer in the experimental environment.

### C. OPTIMIZED PARAMETER EXTRACTION FOR HEFNER MODEL

In order to obtain better simulation results, a two-step parameter extraction approach is used in this article with formal optimization. This procedure utilizes empirical formula to estimate the initial parameters, which offer a suitable range for optimization in the second step, making the optimization

**TABLE 4. Results of Optimized Parameter Extraction**

Para.	Description	Initial range	Optimized
$C_{gs}$	Gate-source capacitance (nF)	(50, 100)	68
$L_c$	Common emitter inductance (nH)	(1, 10)	5.4
$L_g$	Gate inductance (nH)	(0.1, 1)	0.5
$I_{sene}$	Emitter electron saturation current (pA)	( $10^{-2}$ , $10^{-1}$ )	$2 \times 10^{-2}$
$C_O$	Parasitic capacitance (nF)	(0.1, 1)	0.2
$\tau_{HL1}$	Temperature coefficient of $\tau_{HL}$	(1, 5)	2.3
$V_{T1}$	Temperature coefficient of $V_T$	(-0.03, 0)	-0.012
$K_{p1}$	Temperature coefficient of $K_{psat}$ and $K_{plin}$	(0, 1)	0.8

process more manageable. Compared with [29], the optimization process in this part is more user-friendly since the Hefner model has already been coded. Additionally, the MATLAB optimization toolbox is utilized to expedite this process, which is outlined below:

- 1) Determine the parameters and value ranges that need to be optimized, e.g., common emitter inductance  $L_c$ .
- 2) Based on the MATLAB script compiled in Section II, define an optimization function  $f(p_1, p_2, p_3 \dots)$ , in which parameters  $p_1, p_2, p_3 \dots$  are independent of temperature;

$$f(p_1, p_2, p_3 \dots) = \left(\frac{E_{on}}{E_{on}^{25^\circ\text{C}}} - 1\right)^2 + \left(\frac{E_{off}}{E_{off}^{25^\circ\text{C}}} - 1\right)^2 + \left(\frac{t_r}{t_r^{25^\circ\text{C}}} - 1\right)^2 + \left(\frac{t_f}{t_f^{25^\circ\text{C}}} - 1\right)^2 \quad (17)$$

- 3) After confirming the parameters of the second step, define a new optimization function  $f(p_1, p_2, p_3 \dots)$ , in which parameters  $p_1, p_2, p_3 \dots$  are dependent of temperature. In addition, regarding materials, such as the temperature coefficient of silicon [30], details will not be described here.

$$f(p_1, p_2, p_3 \dots) = \left(\frac{E_{on}}{E_{on}^{150^\circ\text{C}}} - 1\right)^2 + \left(\frac{E_{off}}{E_{off}^{150^\circ\text{C}}} - 1\right)^2 + \left(\frac{t_r}{t_r^{150^\circ\text{C}}} - 1\right)^2 + \left(\frac{t_f}{t_f^{150^\circ\text{C}}} - 1\right)^2 \quad (18)$$

Where the reference values of electrothermal stress, e.g.,  $E_{on}^{25/150^\circ\text{C}}$ ,  $E_{off}^{25/150^\circ\text{C}}$ ,  $t_r^{25/150^\circ\text{C}}$  and  $t_f^{25/150^\circ\text{C}}$ , can all be found in the datasheet. Through the above process, the results of optimized parameters are shown in Table 4.

### D. VALIDATION ON ACCURACY

To verify the accuracy of the re-expressed Hefner model in Section II that incorporated with the optimized parameters, an experimental setup is built based on the double-pulse test

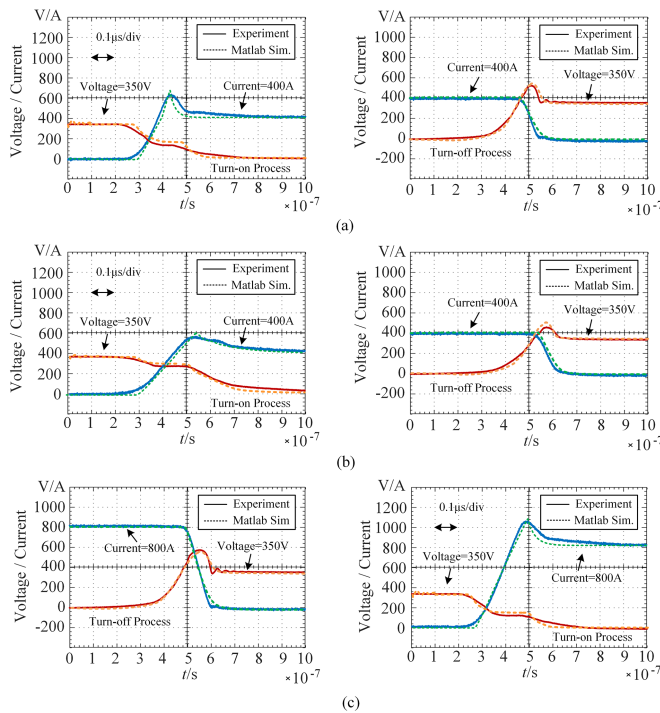


**FIGURE 4.** Comparison between the electrical stress derived from the double pulse test and the re-expressed Hefner model. (a)  $T_j = 25\text{ }^\circ\text{C}$ ,  $U_{dc} = 350\text{ V}$ ,  $I_o = 400\text{ A}$ . (b)  $T_j = 25\text{ }^\circ\text{C}$ ,  $U_{dc} = 350\text{ V}$ ,  $I_o = 800\text{ A}$ . (c)  $T_j = 135\text{ }^\circ\text{C}$ ,  $U_{dc} = 350\text{ V}$ ,  $I_o = 800\text{ A}$ .

**TABLE 5.** Key Parameters of the Experimental Platform

Items	Values (Units)	Items	Values (Units)
Load inductor	109 $\mu\text{H}$	Differential probe	SI-9010 (75MHz)
Capacitor	350 $\mu\text{F}$	Current Probe	CWTUM 6B (30 MHz)
module	FS820R08A6P2B	Oscilloscope	HDO6054 (500 MHz)

principle, as shown in Fig. 4. The parameters of experimental platform are provided in Table 5, in which the gate voltage ( $-20\sim 20\text{ V}$ ), gate resistance, tested voltage ( $100\sim 5000\text{ V}$ ), tested current ( $100\sim 4000\text{ A}$ ) and tested junction temperature can be adjusted by the PC. After testing, the stray inductance of the commutation circuit in the double test platform can be calculated, that is,  $L_c$  set as  $25\text{ nH}$  in the circuit simulation. Besides, other parameters between the proposed circuit simulation and the experiment conditions are consistent, e.g., turn-on and turn-off gate resistance are set as  $2.5/5.5\ \Omega$ , which has been detailed introduced in [31].

Fig. 4(a) presents a comparison of voltage and current waveforms during the turn-on and turn-off processes of the IGBT device at a tested current, voltage and temperature of  $400\text{ A}$ ,  $350\text{ V}$  and  $25\text{ }^\circ\text{C}$ , respectively. The comparison results show that the device experiences maximum current stress during the turn-on process, reaching about  $605\text{ A}$ , while

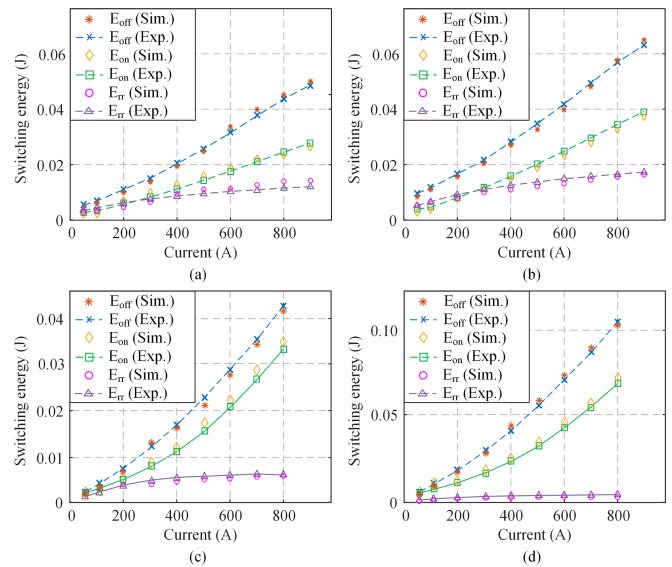


**FIGURE 5.** Comparison between the switching energy derived from the double pulse test and Hefner model. (a)  $T_j = 25\text{ }^\circ\text{C}$ ,  $U_{dc} = 400\text{ V}$ ,  $R_{gon}/R_{goff} = 2.5\ \Omega/5.5\ \Omega$ . (b)  $T_j = 135\text{ }^\circ\text{C}$ ,  $U_{dc} = 400\text{ V}$ ,  $R_{gon}/R_{goff} = 2.5\ \Omega/5.5\ \Omega$ . (c)  $T_j = 25\text{ }^\circ\text{C}$ ,  $U_{dc} = 300\text{ V}$ ,  $R_{gon}/R_{goff} = 2.5\ \Omega/5.5\ \Omega$ . (d)  $T_j = 25\text{ }^\circ\text{C}$ ,  $U_{dc} = 400\text{ V}$ ,  $R_{gon}/R_{goff} = 5\ \Omega/10\ \Omega$ .

the maximum voltage stress occurs during device turn-off, at around  $510\text{ V}$ . The error between the circuit simulation and experimental results is less than  $5\%$ . In addition, Fig. 4(b) and (c) show the comparison results of the IGBT voltage and current waveforms during turn-on and turn-off processes at a different temperature of  $135\text{ }^\circ\text{C}$  or a different tested current of  $800\text{ A}$ , which demonstrates that the proposed re-expressed Hefner model in this article can effectively describe the dynamic switching transient of the IGBT device under various system conditions. Further, Fig. 5 presents a comparison between the switching energy obtained from the re-expressed model and experimental data, which confirms the accuracy of the model under various operating conditions. Thus, by using additional scripts for batch operations, the re-expressed model enables obtaining the accurate training data for the ANN models with a high efficiency.

#### IV. ELECTROTHERMAL EVALUATION APPROACH COMBINED WITH ANN MODEL

In this section, the implementation of ANNs in MATLAB is presented, which includes the process of generation and the integration with the thermal network model in Simulink.

##### A. DESCRIPTION OF ANN MODEL

Using the precise electrothermal information provided by the physical model that has been validated in Section III, ANN models are adopted in this part to alleviate the excessive computational burden resulting from the requirement to solve nonlinear equations in real-time during system-level circuit simulations.

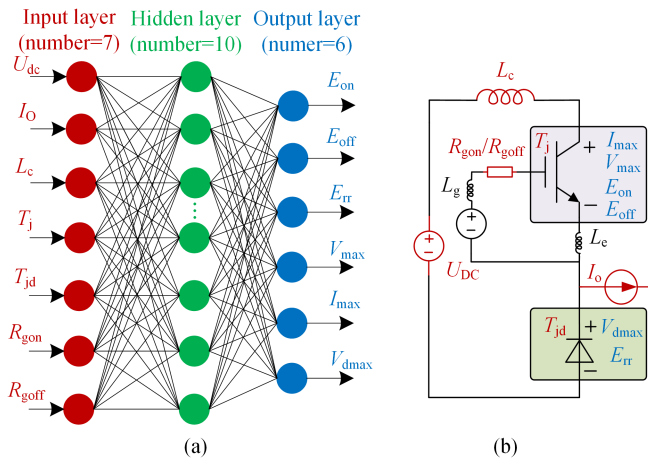


**FIGURE 6.** ANN model for electrothermal stress evaluation. (a) Structure of ANN model. (b) Characteristics parameters used for training ANN model.

In general, ANN models are designed to simulate the biological processes of the human brain. By training with existing data, they can learn and identify internal patterns and approximate data laws. Furthermore, with an appropriate number of neurons in the hidden layer, ANN models have powerful mapping capabilities, which make them capable of accurately predicting data even under unknown conditions. Therefore, a two-layer feed-forward ANN is adopted in this article, which consists of 10 sigmoid hidden layer neurons and 6 linear output neurons, as shown in Fig. 6(a). In practice, networks with different layers can be tried and compared to find the most suitable network structure for a particular problem. In addition, the characteristics parameters used for training the ANN model can refer to Fig. 6(b). For the input layer, the characteristics parameters are provided by system and parasitic characteristics, e.g.,  $L_c$ ,  $R_{gon}$ ,  $R_{goff}$ ,  $I_o$ ,  $U_{dc}$ ,  $T_j$  and  $T_{jd}$ . For the output layer, the characteristics parameters of electrothermal stress include the switching energy ( $E_{on}$ ,  $E_{off}$ ,  $E_{rr}$ ) of IGBT and Diode device, maximum current stress ( $I_{max}$ ) and maximum voltage stress ( $U_{max}$ ).

A total of 1400 datasets were utilized to train the ANN using the backpropagation algorithm, e.g., Levenberg-Marquardt (LM). To measure the generalization ability of the neural network, 300 sets of data were used, and training was stopped when there was no further improvement in generalization ability. Additionally, the remaining 300 datasets were utilized to test the performance of the trained ANNs. Fig. 7 presents the training processes for three sets of ANN models, including switching energy, maximum current stress and voltage stress of IGBT and Diode device, respectively. The mean squared error of the three ANN models are 0.0128, 31.8635 and 11.5128. As shown in Fig. 7(a), the root errors between targets and outputs are kept within a small interval, such as  $-0.3198$  and  $0.3631$ , when compared to the curve of zero error, indicating that overfitting did not occur. In statistical analysis, the coefficient of determination  $R^2$  is commonly used to evaluate predictive performance of the ANN model,

**TABLE 6.** Parameters of the Thermal Network Model

Device	Parameters	Order ( $i$ )			
		1	2	3	4
IGBT	$R_i$	0.005	0.05	0.065	0.02
	$\tau_i$	0.001	0.03	0.25	1.5
Diode	$R_i$	0.015	0.1	0.065	0.02
	$\tau_i$	0.001	0.03	0.25	1.5

where a higher value represents better prediction. In this study, the  $R^2$  values of the model are all above 0.999.

## B. IMPLEMENTATION OF ELECTROTHERMAL STRESS EVALUATION

After the training and evaluation of ANN model is finished, a function block can be generated in Simulink. As shown in Fig. 8, this function block is able to be integrated into a system-level electrothermal simulation, enabling accurate description of the dynamic and static behaviors of the IGBT device for a given gate drive signal. It is worth noting that the ideal IGBT models are adopted in the system-level circuit simulation to obtain the systems parameters in real time, e.g.,  $U_{dc}$  and  $I_o$ , which realizes higher simulation efficiency. In addition, the process of enabling the stress calculation is also provided in Fig. 8, which depends on the change of the driving signal. For the dynamic behavior, For the dynamic behavior, the trained ANN model accurately captures the significant characteristics of the switching transient. For the static behavior, assuming that the device current  $I_o$  is positive, the conduction energy losses of IGBT and Diode in one switching cycle can be calculated with (19) [32]. This allows for a comprehensive analysis of the overall power loss of the system and helps to optimize the design.

$$\begin{cases} E_{con}(I_o, T_j) = \int_{t_{on}}^{t_{off}} I_o \cdot U_{ce}(I_o, T_j) dt \\ E_{cond}(I_o, T_j) = \int_{t_{off}}^{t_{on}+T_s} I_o \cdot U_f(I_o, T_{jd}) dt \end{cases} \quad (19)$$

Where  $U_{ce}$  and  $U_f$  are the output characteristics of IGBT and Diode provided in the datasheet, respectively. The action time of  $t_{on}$  and  $t_{off}$  is determined by the driving signal. Therefore, the averaged energy losses of IGBT or Diode device in one switching cycle can be calculated by (20).

$$\begin{cases} P_{IGBT} = \frac{E_{on} + E_{off} + E_{con}}{T_s} \\ P_{Diode} = \frac{E_{rr} + E_{cond}}{T_s} \end{cases} \quad (20)$$

Additionally, the junction temperature  $T_j$ ,  $T_{jd}$  are obtained by transferring the power losses to the 4-order thermal network, which is provided in the datasheet with a series of value of thermal resistances ( $R$ ) and time-constants ( $\tau$ ) shown in Table 6. Further, the junction temperature  $T_j$ ,  $T_{jd}$  are fed back to the ANN models as well as the averaged power loss calculation model for a closed loop. In this article, the temperature of heatsink ( $T_h$ ) is used as a reference value of the thermal network, which is set as  $25^\circ\text{C}$ .

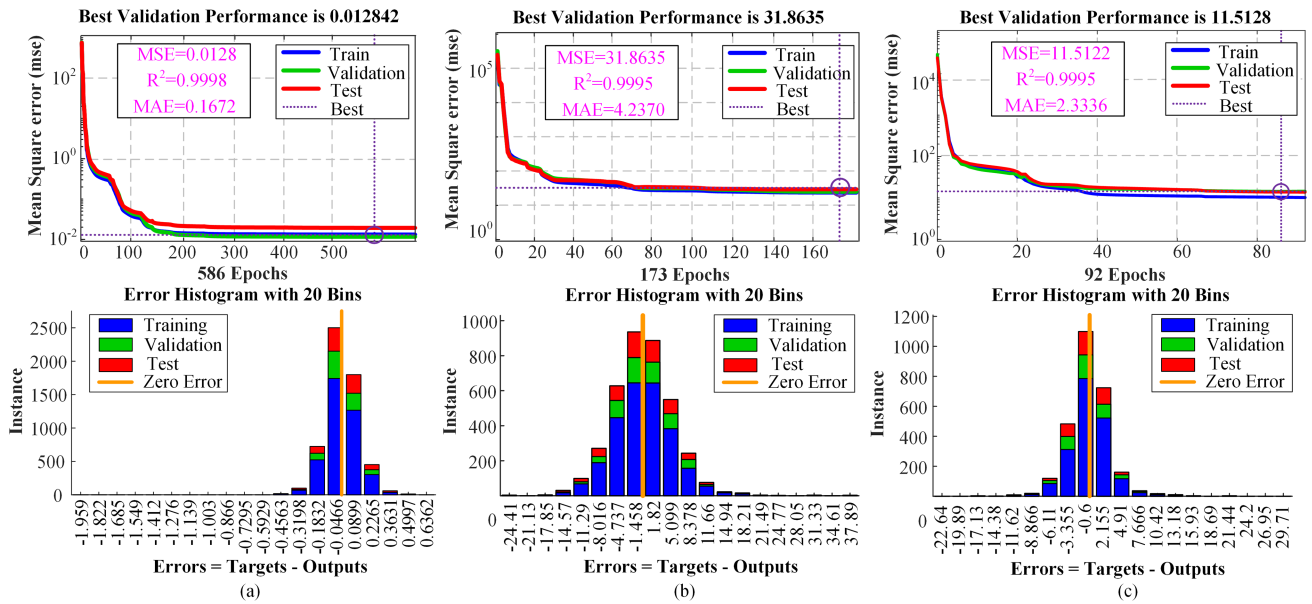


FIGURE 7. MSEs obtained from the trained ANN models. (Top: best validation performance, bottom: distribution of error). (a) Switching energy of IGBT and Diode device. (b) Maximum current and voltage stress of IGBT device. (c) Maximum voltage stress of Diode device.

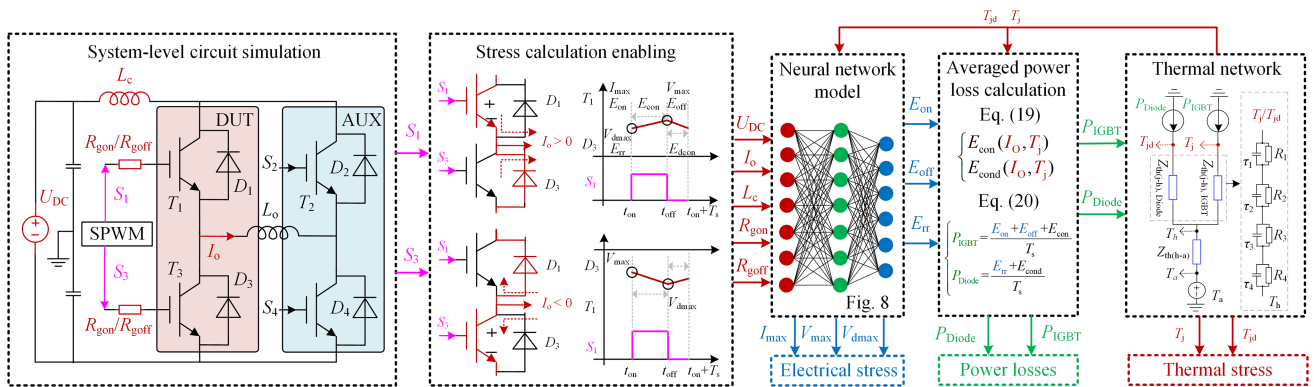


FIGURE 8. Detailed simulation process for proposed electrothermal stress evaluation approach of IGBT modules.

### C. ELECTROTHERMAL STRESS VALIDATION WITH SABER

To verify the effectiveness of the proposed electrothermal stress evaluation approach that implemented in MATLAB/Simulink, an electrothermal simulation with a same test circuit is also built in Saber environment, which provides convincing conclusions. In addition, the parameters of the IGBT Hefner model used in Saber are the same as those selected in this article, see Tables 3 and 4.

The comparison results have been divided into electrical stress and thermal stress. The former is shown in Fig. 9 which contains the information of maximum current stresses and maximum voltage stresses under different operating conditions, e.g., DC-bus voltage  $U_{dc}$  and arm output current  $I_O$ . The results show that the envelopes of voltage and current stress displayed in Simulink have a high consistency with the real-time simulation waveform of Saber. The predicted errors of the maximum voltage and current stresses shown are all

less than 2%, which demonstrates the high accuracy of the proposed approach in electrical stress evaluation.

In addition, Fig. 10 provides the thermal stress comparison results of these two models under different operating conditions, e.g., DC-bus voltage  $U_{dc}$ , arm output current  $I_O$  and gate resistance  $R_{gon}/R_{goff}$ . The junction temperatures of IGBT and Diode devices reach their maximum values during the positive and negative half cycles of the bridge arm output current, respectively. It can be seen that with the operating conditions changing, the thermal stresses obtained by the proposed approach implemented in Simulink still trace the simulation results of Saber well, and the maximum junction temperature prediction errors are kept within 2.5%.

Moreover, the improvement of simulation efficiency is also studied in this section, which implies lower hardware cost requirements. In the electrical stress evaluation shown in Fig. 9 (the total simulation time is 0.2 s), the switching frequency



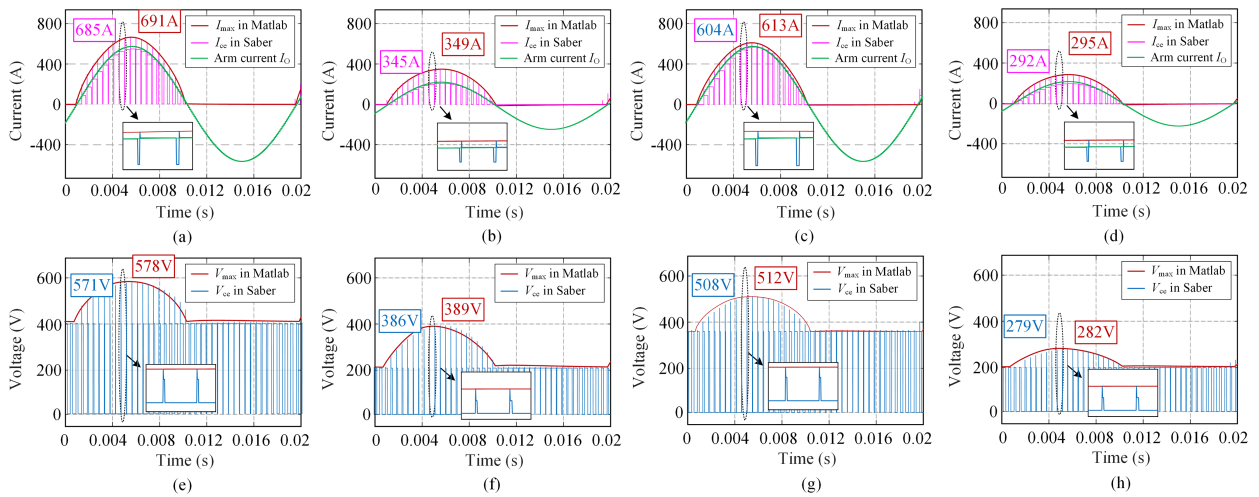


**FIGURE 9.** Validation results of the electrical stresses. Maximum current stresses for (a)  $U_{dc} = 400V$ ,  $I_o = 400A$ , (b)  $U_{dc} = 400V$ ,  $I_o = 150A$ , (c)  $U_{dc} = 200V$ ,  $I_o = 400A$  and (d)  $U_{dc} = 200V$ ,  $I_o = 150A$ . Maximum voltage stresses for (e)  $U_{dc} = 400V$ ,  $I_o = 400A$ , (f)  $U_{dc} = 200V$ ,  $I_o = 400A$ , (g)  $U_{dc} = 400V$ ,  $I_o = 150A$  and (h)  $U_{dc} = 200V$ ,  $I_o = 150A$ .

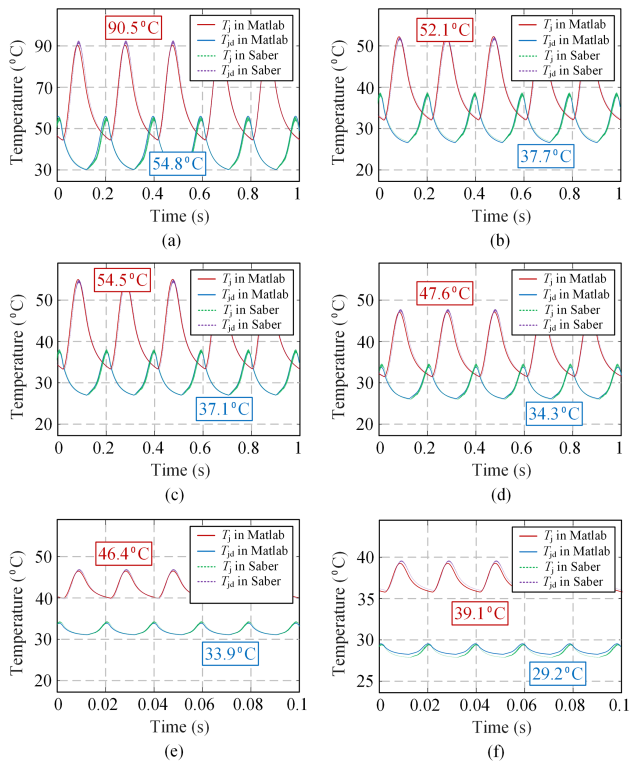


**FIGURE 10.** Validation results of the thermal stresses. (a)  $U_{dc} = 400V$ ,  $I_o = 400A$ ,  $R_{gon}/R_{goff} = 2.5 \Omega/5.5 \Omega$ ,  $f_o = 5Hz$ ,  $f_{sw} = 1000Hz$ . (b)  $U_{dc} = 400V$ ,  $I_o = 200A$ ,  $R_{gon}/R_{goff} = 2.5 \Omega/5.5 \Omega$ ,  $f_o = 5Hz$ ,  $f_{sw} = 1000Hz$ . (c)  $U_{dc} = 200V$ ,  $I_o = 400A$ ,  $R_{gon}/R_{goff} = 2.5 \Omega/5.5 \Omega$ ,  $f_o = 5Hz$ ,  $f_{sw} = 1000Hz$ . (d)  $U_{dc} = 200V$ ,  $I_o = 200A$ ,  $R_{gon}/R_{goff} = 5 \Omega/10 \Omega$ ,  $f_o = 5Hz$ ,  $f_{sw} = 1000Hz$ . (e)  $U_{dc} = 400V$ ,  $I_o = 150A$ ,  $R_{gon}/R_{goff} = 2.5 \Omega/5.5 \Omega$ ,  $f_o = 50Hz$ ,  $f_{sw} = 2000Hz$ . (f)  $U_{dc} = 200V$ ,  $I_o = 150A$ ,  $R_{gon}/R_{goff} = 2.5 \Omega/5.5 \Omega$ ,  $f_o = 50Hz$ ,  $f_{sw} = 2000Hz$ .

of IGBT device is set to 2000 Hz. In Saber environment, the simulation step size is defined as 20 ns, and it takes about 18 mins to complete the whole circuit simulation. However, the proposed approach only needs 6 s to complete the

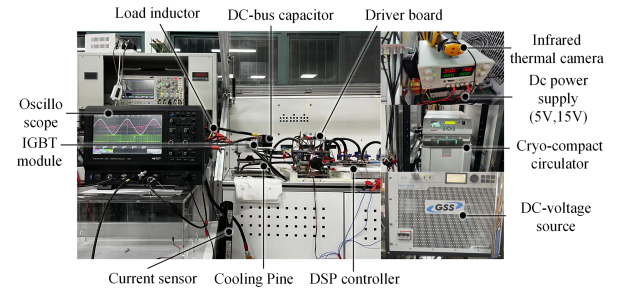


**FIGURE 11.** Experimental setup.

simulation when the simulation step size is set as  $2 \mu s$ , and the simulation efficiency is increased by about 180 times. In the thermal stress evaluation, due to the large thermal time constant, it takes longer time to reach the thermal steady-state condition in which the highest junction temperature appears. For instance, the total simulation time implemented in Fig. 10 is set as 10 s, and the junction temperature data of the last one second is regarded as the steady-state data. As mentioned before, due to inconsistent electrical and thermal time scales, the simulation efficiency of Saber faces severe challenges, and it takes hours to evaluate the thermal behaviors. However, the proposed approach enables reducing the simulation time to less than 5 mins, which helps designers to quickly evaluate the thermal stresses of IGBT and Diode. In order to further improve the accuracy of thermal stress evaluation, future work will focus on considering the thermal coupling effect between different devices caused by compact packaging structure and verify its effectiveness by implementing detailed experiments.

#### D. ELECTROTHERMAL STRESS VALIDATION WITH EXPERIMENTS

To further verify the effectiveness of the proposed method, an experimental configuration was implemented, as shown in Figs. 8 and 11. The experimental setup comprises an

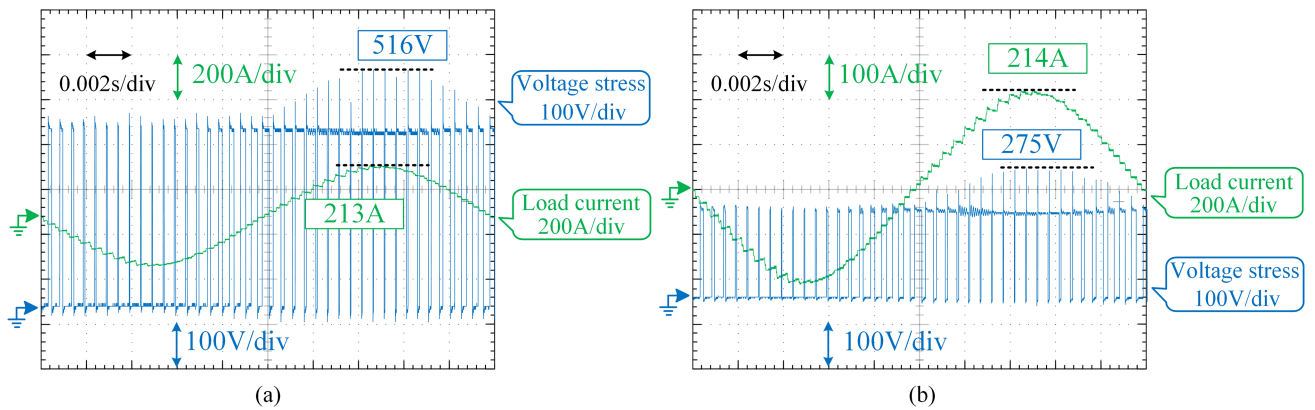


FIGURE 12. Experimental results for voltage stresses. (a)  $U_{dc} = 400V, i_L = 150A$  and (b)  $U_{dc} = 200V, i_L = 150A$ .

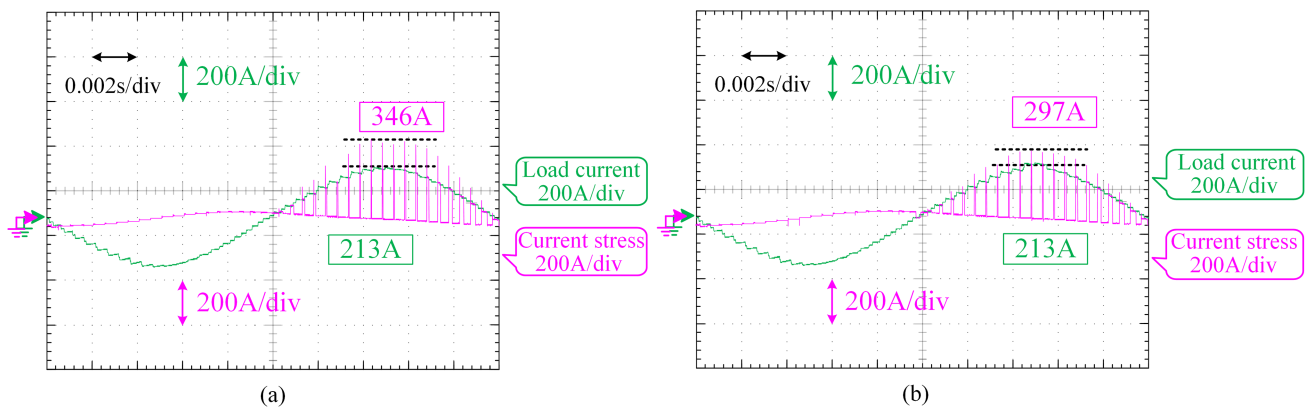


FIGURE 13. Experimental results for current stresses. (a)  $U_{dc} = 400V, i_L = 150A$  and (b)  $U_{dc} = 200V, i_L = 150A$ .

TABLE 7. Key Parameters of the Experimental Platform

Items	Values (Units)	Items	Values (Units)
Load inductor	314 $\mu$ H, 160A	Differential probe	SI-9010 (75MHz)
Capacitor	4800 $\mu$ F, 1200V	Current Probe	TCP303 (15MHz)
Module	FS820R08A6P2B	IR camera	FLK-TI450 (60Hz)
Switching frequency	2 kHz	Output frequency	50 Hz
dc-voltage source	1000V/40A	Cooling system	Water, Julabo CF41

H-bridge inverter (two phases of an IGBT module), a water-cooling system, and an infrared (IR) thermal camera. The specific setup parameters are presented in Table 7. A total of two experiments have been conducted under various operational circumstances: (1)  $U_{dc} = 400V, i_L = 150A$  and (2)  $U_{dc} = 200V, i_L = 150A$ . The experimental results pertaining to the voltage stress are depicted in Fig. 12. Upon comparing the simulation results of the corresponding working conditions shown in Fig. 8, the maximum error of the proposed

method in voltage stress is found to be below 1.5%. In addition, In addition, Fig. 13 shows the experimental results of current stresses. By analyzing the comparison results with the related simulation results, it can be seen that the maximum error of the proposed model for predicting the current stress is less than 1%, which fully verifies the accuracy of the proposed model.

For the analysis of thermal stresses, due to the low sampling frequency of the infrared camera, the junction temperature swing due to power fluctuations is difficult to observe. As a result, the junction temperatures of the steady-state condition are recorded for a period of time. Then, the frame with the highest junction temperature is selected as the infrared imaging results for comparison with the simulation results, which have been provided in Fig. 14. The results show that the maximum error between the proposed model and experiments is approximately 2.5%, and it tends to increase with higher load currents. This discrepancy is primarily attributed to the adoption of a one-dimensional (1-D) thermal network model in this study, which aims to simplify modeling complexity and enhance computational efficiency. However, the IGBT module (FS820R08A6P2B) under study case employs a multi-chip

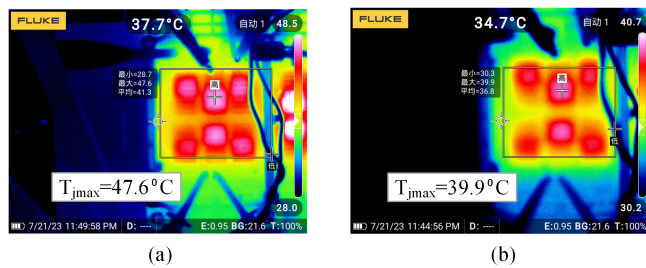


**FIGURE 14.** Experimental results for thermal stresses. (a)  $U_{dc} = 400V$ ,  $I_L = 150A$  and (b)  $U_{dc} = 200V$ ,  $I_L = 150A$ .

parallel structure to enhance its current-carrying capacity, leading to three-dimensional (3-D) heat conduction effects. This highlights the importance of implementing a 3D thermal network model for multi-chip modules, which is also the content that needs to be improved in the follow-up of this article.

## V. CONCLUSION

This article proposes an improved electrothermal stress evaluation approach combining accurate physical models with ANN that has strong nonlinear mapping capability. The proposed approach exhibits excellent performance in both simulation accuracy and efficiency. The main work and contributions of this article can be summarized as follows:

- 1) The MATLAB re-expression of the physics-based Hefner model enables batch processing of electrothermal stress data, overcoming the limitation of existing commercial software (Saber) for large-scale data acquisition. This approach effectively generates training data for ANN model.
- 2) To enhance model accuracy, an automatic parameter optimization process based on the two-step parameter extraction is proposed in this article, which combines with the re-expressed MATLAB script of describing the transient switching process of IGBT modules. The switching transient error between simulation and double-pulse experiments is kept within 5%, and excellent agreement is observed in the comparison of switching energies.
- 3) To realize the optimal trade-off between the simulation accuracy and efficiency, the electrothermal stress evaluation method is implemented in Simulink, which adopts ANN models to describe the switching transients, e.g., energy, current and voltage overshoot. Its validity has been verified by Saber, and the errors of both transient electrical stress and steady-state thermal stress are less than 2.5%. In addition, its simulation efficiency is increased by about 180 times than that of Saber, which helps quickly traverse more operating conditions during the design phase. Finally, experimental results under two sets of working conditions validate the proposed model's accuracy in predicting voltage and current stress, with a maximum error of less than 1.5%.

## REFERENCES

- [1] H. Wang and F. Blaabjerg, "Power electronics reliability: State of the art and outlook," *IEEE J. Emerg. Sel. Topics Power Electron.*, vol. 9, no. 6, pp. 6476–6493, Dec. 2021.
- [2] H. Wang, M. Liserre, and F. Blaabjerg, "Toward reliable power electronics: Challenges, design tools, and opportunities," *IEEE Ind. Electron. Mag.*, vol. 7, no. 2, pp. 17–26, Jun. 2013.
- [3] S. Yang, A. T. Bryant, P. Mawby, D. Xiang, L. Ran, and P. Tavner, "An industry-based survey of reliability in power electronic converters," *IEEE Trans. Ind. Appl.*, vol. 47, no. 3, pp. 1441–1451, May/Jun. 2011.
- [4] A. R. Hefner, "Modeling buffer layer IGBTs for circuit simulation," *IEEE Trans. Power Electron.*, vol. 10, no. 2, pp. 111–123, Mar. 1995.
- [5] A. R. Hefner, "Device models, circuit simulation, and computer-controlled measurements for the IGBT," in *Proc. IEEE Workshop Comput. Power Electron.*, 1990, pp. 233–243.
- [6] A. R. Hefner and D. M. Diebolt, "An experimentally verified IGBT model implemented in the Saber circuit simulator," *IEEE Trans. Power Electron.*, vol. 9, no. 5, pp. 532–542, Sep. 1994.
- [7] K. Sheng, S. J. Finney, and B. W. Williams, "A new analytical IGBT model with improved electrical characteristics," *IEEE Trans. Power Electron.*, vol. 14, no. 1, pp. 98–107, Jan. 1999.
- [8] S. Ji, Z. Zhao, T. Lu, L. Yuan, and H. Yu, "HVIGBT physical model analysis during transient," *IEEE Trans. Power Electron.*, vol. 28, no. 5, pp. 2616–2624, May 2013.
- [9] I. T. AG, "Simulation model -infineon technologies," Dec. 2021. Accessed: Apr. 11, 2023. [Online]. Available: <https://www.infineon.com/cms/en/design-support/finder-selection-tools/product-finder/simulation-model/>
- [10] "Mitsubishi electric global website," *MITSUBISHI ELECTRIC Global Website*. Mar. 2023. Accessed: Jun. 15, 2023. [Online]. Available: <https://www.mitsubishielectric.com/en/index.html>
- [11] "Support: Drivers, manuals, tutorials | Toshiba business," May 2023. Accessed: Jun. 11, 2023. [Online]. Available: <https://business.toshiba.com/support/#downloads>
- [12] "LTspice information center | analog devices," Jan. 2023. Accessed: Jun. 11, 2023. [Online]. Available: <https://www.analog.com/en/design-center/design-tools-and-calculators/ltspice-simulator.html>
- [13] "Electronic circuit optimization & simulation | cadence PSpice | PSpice," Mar. 2020. Accessed: Apr. 23, 2023. [Online]. Available: <https://www.pspice.com/>
- [14] "SIMetrix circuit design and simulation," Jan. 2023. Accessed: Apr. 15, 2023. [Online]. Available: <https://www.simetrix.co.uk>
- [15] "Power electronics simulation software | Ansys," Jan. 2023. Accessed: Apr. 11, 2023. [Online]. Available: <https://www.ansys.com/applications/power-electronics>
- [16] B. Shi, Z. Zhao, and Y. Zhu, "Piecewise analytical transient model for power switching device commutation unit," *IEEE Trans. Power Electron.*, vol. 34, no. 6, pp. 5720–5736, Jun. 2019.
- [17] Y. Zhu, Z. Zhao, B. Shi, and Z. Yu, "Discrete state event-driven framework with a flexible adaptive algorithm for simulation of power electronic systems," *IEEE Trans. Power Electron.*, vol. 34, no. 12, pp. 11692–11705, Dec. 2019.
- [18] "Power electronics simulation software | Ansys," Sep. 2022. Accessed: Apr. 11, 2023. [Online]. Available: <https://www.ansys.com/applications/power-electronics>
- [19] N.-C. Sintamarean, F. Blaabjerg, H. Wang, F. Iannuzzo, and P. de Place Rimmen, "Reliability oriented design tool for the new generation of grid connected PV-inverters," *IEEE Trans. Power Electron.*, vol. 30, no. 5, pp. 2635–2644, May 2015.
- [20] B. Shi, Z. Zhao, Y. Jiang, and Y. Zhu, "Multi-time scale transient models for power semiconductor devices (Part I: Switching characteristics and transient modeling)," *Diangong Jishu Xuebao/Trans. China Electrotechnical Soc.*, vol. 32, pp. 16–24, Jun. 2017.
- [21] B. Liu, F. Xiao, Y. Luo, Y. Huang, and Y. Xiong, "A multi-timescale prediction model of IGBT junction temperature," *IEEE J. Emerg. Sel. Topics Power Electron.*, vol. 7, no. 3, pp. 1593–1603, Sep. 2019.
- [22] K. Ma and F. Blaabjerg, "Multi-timescale modelling for the loading behaviours of power electronics converter," in *Proc. IEEE Energy Convers. Congr. Expo.*, 2015, pp. 5749–5756.
- [23] Y. Wang et al., "An artificial neural network model for electro-thermal effect affected hot carrier injection reliability in 14-nm FinFETs," *IEEE Trans. Microw. Theory Techn.*, vol. 70, no. 11, pp. 4827–4834, Nov. 2022.

- [24] C. L. Ma and P. O. Lauritzen, "A simple power diode model with forward and reverse recovery," *IEEE Trans. Power Electron.*, vol. 8, no. 4, pp. 342–346, Oct. 1993.
- [25] C. L. Ma, P. O. Lauritzen, and J. Sigg, "Modeling of power diodes with the lumped-charge modeling technique," *IEEE Trans. Power Electron.*, vol. 12, no. 3, pp. 398–405, May 1997.
- [26] I. T. AG, "FS820R08A6P2B | 750 V, 820 A sixpack automotive qualified IGBT module - Infineon technologies," Jun. 2023. Accessed: Jun. 15, 2023. [Online]. Available: <https://www.infineon.com/cms/en/product/power/igbt/automotivequalified-igbt-automotive-igbt-coolsic-mosfet-modules>
- [27] B. J. Baliga, *Fundamentals of Power Semiconductor Devices*. Berlin, Germany: Springer, 2019.
- [28] C. Gomez Suarez, P. Diaz Reigosa, F. Iannuzzo, I. Trintis, and F. Blaabjerg, "Parameter extraction for PSpice models by means of an automated optimization tool—An IGBT model study case," in *Proc. IEEE Int. Exhib. Conf. Power Electron., Intell. Motion, Renewable Energy Energy Manage.*, 2016, pp. 1–8.
- [29] A. T. Bryant, X. Kang, E. Santi, P. R. Palmer, and J. L. Hudgins, "Two-step parameter extraction procedure with formal optimization for physics-based circuit simulator IGBT and p-i-n diode models," *IEEE Trans. Power Electron.*, vol. 21, no. 2, pp. 295–309, Mar. 2006.
- [30] A. R. Hefner, "A dynamic electro-thermal model for the IGBT," *IEEE Trans. Ind. Appl.*, vol. 30, no. 2, pp. 394–405, Mar./Apr. 1994.
- [31] A. Zhu, H. Gao, Y. Xia, H. Luo, W. Li, and X. He, "Adaptive stray inductance extraction algorithm using linear regression for power module with high noise immunity and accuracy," *CPSS Trans. Power Electron. Appl.*, vol. 7, no. 2, pp. 176–185, Jun. 2022.
- [32] Y. Lu, E. Xiang, A. Zhu, H. Luo, H. Yang, and R. Zhao, "Mission-profile-based reliability evaluation of IGBT modules for wide-speed range electric vehicle drive using fast multi-step mapping simulation strategy," *IEEE J. Emerg. Sel. Topics Power Electron.*, early access, Jul. 27, 2023, doi: [10.1109/JESTPE.2023.3299464](https://doi.org/10.1109/JESTPE.2023.3299464).



**YIPING LU** (Student Member, IEEE) received the B.S. degree in electrical engineering in 2019 from Zhejiang University, Hangzhou, China, where he is currently working toward the Ph.D. degree in electrical engineering.

His research interests include high performance motor torque control in electric vehicles and reliability assessment for high-power modules.



**ENYAO XIANG** received the B.S. degree from the Department of Electrical Engineering, Hefei University of Technology, Hefei, China, in 2021. He is currently working toward the master's degree in electrical engineering with Zhejiang University, Hangzhou, China.

His research interests include reliability prediction and aging condition monitoring for high-power modules.



**ANKANG ZHU** received the B.Sc. degree in electrical engineering from the Nanjing University of Aeronautics and Astronautics, Nanjing, China, in 2018. He is currently working toward the Ph.D. degree with the College of Electrical Engineering, Zhejiang University, Hangzhou, China.

His research focuses on robustness and reliability of power devices.



**HONGYI GAO** received the B.Sc. degree in electrical engineering from Hunan University, Changsha, China, in 2019. He is currently working toward the Ph.D. degree with the College of Electrical Engineering, Zhejiang University, Hangzhou, China.

His research focuses on the design and reliability of power devices packaging.



**HAOZE LUO** (Senior Member, IEEE) received the B.S. and M.S. degrees from the Department of Electrical Engineering, Hefei University of Technology, Hefei, China, in 2008 and 2011, respectively, and the Ph.D. degree from Zhejiang University, Hangzhou, China, in 2015. From 2015, he was a Visiting Researcher with Newcastle University, Newcastle upon Tyne, U.K. From 2015 to 2018, he was a Postdoc with the Department of Energy Technology, Aalborg University, Aalborg, Denmark. From 2018 to 2019, he was a Senior

R&D Engineer with Dynex Power Inc., Lincoln, U.K. Since 2019, he has been a Research Fellow with Zhejiang University.

His research focuses on reliability assessment for high-power modules.



**HUAN YANG** (Member, IEEE) received the B.Sc. and Ph.D. degrees in electrical engineering and its automation and electrical engineering from Zhejiang University, Hangzhou, China, in 2003 and 2008, respectively. He is currently the Vice Director of the Zhejiang Provincial Key Laboratory of Electrical Machine Systems.

From 2009 to 2011, he was a Postdoctoral Fellow with Zhejiang University. In 2011, he became a Faculty Member with Zhejiang University, and became an Associate Professor of electrical engineering in 2012. From 2012 to 2013, he conducted joint research with Fuji Electric Company, Ltd. as the Oversea Researcher of New Energy and Industrial Technology Development Organization, Tokyo, Japan.

His research interests include distribution generation and microgrids, high-performance motor systems, and smart power distribution equipment.



**RONGXIANG ZHAO** (Member, IEEE) received the B.S., M.S., and Ph.D. degrees in electrical engineering from Zhejiang University, Hangzhou, China, in 1984, 1987, and 1991, respectively.

He became a Faculty Member with Zhejiang University, in 1991, and was promoted as an Associate Professor, in 1994. Since 1997, he has been a Full Professor with the College of Electrical Engineering, Zhejiang University, where he was the Vice Dean of the College of Electrical Engineering. He is currently the Director of the National Engineering Research Center for Applied Power Electronics of China, Zhejiang University. His research interests include renewable energy generation, motor control, and energy storage and its applications.

Dr. Zhao was the recipient of six Scientific and Technological Achievements Awards from Zhejiang Provincial Government and one Science and Technology Progress Award from the State Educational Ministry of China.

Dr. Zhao was the recipient of six Scientific and Technological Achievements Awards from Zhejiang Provincial Government and one Science and Technology Progress Award from the State Educational Ministry of China.